Yolk syncytial layer formation is a failure of cytokinesis mediated by Rock1 function in the early zebrafish embryo

Lee-Thean Chu[1],*, Steven H. Fong[1],*, Igor Kondrychyn[1], Siau Lin Loh[1], Zhanrui Ye[1] and Vladimir Korzh[1,2],‡

[1]Institute of Molecular and Cell Biology (IMCB), A-STAR (Agency for Science, Technology and Research), 61 Biopolis Drive, Proteos, Singapore 138673
[2]Department of Biological Sciences, National University of Singapore, Singapore 117543

*These authors contributed equally to this work
‡Author for correspondence (vlad@imcb.a-star.edu.sg)

Biology Open

Summary

The yolk syncytial layer (YSL) performs multiple critical roles during zebrafish development. However, little is known about the cellular and molecular mechanisms that underlie the formation of this important extraembryonic structure. Here, we demonstrate by timelapse confocal microscopy of a transgenic line expressing membrane-targeted GFP that the YSL forms as a result of the absence of cytokinesis between daughter nuclei at the tenth mitotic division and the regression of pre-existing marginal cell membranes, thus converting the former margin of the blastoderm into a syncytium. We show that disruption of components of the cytoskeleton induces the formation of an expanded YSL, and identify Rock1 as the regulator of cytoskeletal dynamics that lead to YSL formation.

Our results suggest that the YSL forms as a result of controlled cytokinesis failure in the marginal blastomeres, and Rock1 function is necessary for this process to occur. Uncovering the cellular and molecular mechanisms underlying zebrafish YSL formation offers significant insight into syncytial development in other tissues as well as in pathological conditions.

Introduction

The yolk syncytial layer (YSL) is a multinucleate layer of non-yolky cytoplasm immediately beneath the cellular blastoderm. It is the first lineage-restricted extraembryonic structure to form in the zebrafish embryo (Kimmel et al., 1995). Although it does not contribute cells or nuclei to the embryo, it is nevertheless important for embryonic development (Carvalho and Heisenberg, 2010). It is crucial for induction of the embryonic organizer (Mizuno et al., 1999), early patterning of mesoderm and endoderm (Mizuno et al., 1996; Rodaway et al., 1999), epiboly (Trinkaus, 1993; Solnica-Krezel and Driever, 1994) and cardiac morphogenesis (Sakaguchi et al., 2006). Additionally, the YSL plays a nutritive role during embryonic and larval stages (Walzer and Schönenberger, 1979a; Walzer and Schönenberger, 1979b).

Our understanding of YSL formation is largely limited to descriptive studies. The YSL forms in a similar manner in a number of teleosts: marginal blastomeres undergo a morphogenetic "collapse" upon the yolk cell to form the YSL (Kimmel and Law, 1985; Trinkaus, 1993). In the zebrafish embryo, this occurs at the ninth or tenth cell division (Kimmel and Law, 1985). The final step of cell division is cytokinesis – the division of the cytoplasm into two daughter cells following karyokinesis. Cytokinesis is a highly regulated multistep process (reviewed by Eggert et al., 2006), which involves continuous remodelling of the cytoskeleton and plasma membranes to effect

the necessary changes in cytoarchitecture. Small GTPases of the Rho family, which are molecular switches that control many cytoskeleton-dependent cell functions, have been implicated in this process (Etienne-Manneville and Hall, 2002). Rho kinases (Rocks) are downstream effectors of Rho signalling – activated GTP-bound Rho binds to Rock at its Rho-binding domain, thereby relieving the autoinhibitory loop formed by interaction between the N- and C-termini of Rock (Riento and Ridley, 2003). Although the molecular mechanism underlying cytokinesis has been a matter of intense investigation, the molecular mechanism underlying YSL formation is only just beginning to be elucidated (Takesono et al., 2012). This report demonstrated that solute carrier family 3 member 2 (Slc3a2) inhibits the RhoA/Rock pathway via phosphorylation of c-Src to modulate YSL microtubule dynamics and YSL formation. Here, we show using timelapse confocal microscopy of a transgenic zebrafish line expressing membrane-targeted GFP that the YSL forms as a result of the absence of cytokinesis between marginal daughter nuclei at the tenth mitotic division and the regression of pre-existing marginal cell membranes. Disruption of components of the cytoskeleton by various means, including nocodazole, cytochalasin D and attenuation of Rock function by small molecule inhibitors led to YSL expansion. To define which Rho kinase is responsible for this effect we employed the dominant-negative loss-of-function (LOF) strategy and demonstrated that

LOF of Rock1, but not Rock2, led to YSL expansion. Taken together, these results indicate that the YSL forms as a result of regulated cytokinesis failure of the marginal blastomeres, and attenuation of Rock1 activity is necessary for this process to occur.

Results and Discussion

Microtubule and membrane dynamics in the early zebrafish embryo

The distribution and organization of microtubules in the yolk cell of the early zebrafish embryo have been analysed by immunolabelling (Strähle and Jesuthasan, 1993; Solnica-Krezel and Driever, 1994). In this study, late cleavage and blastula stage embryos were examined by whole-mount immunofluorescence to visualize changes in the organization of yolk cortical microtubules for the period leading to and spanning YSL formation (Fig. 1). From the 32- to 512-cell stage, the
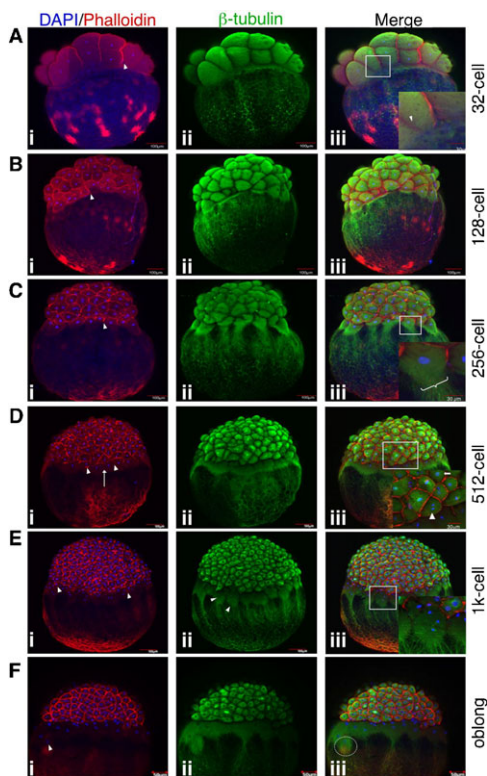
microtubule arrays of the marginal blastomeres extended into the yolk cortex along the animal-vegetal axis (Fig. 1Aii–Dii). Cell borders were evident between marginal blastomeres from the 32- to the 256-cell stage (Fig. 1Ai–Ci, arrowheads). At the 256-cell stage, the yolk cortical microtubules emanated mainly from the central region of the base of the marginal blastomeres (Fig. 1Ciii, inset). At the 512-cell stage (2.75 hpf), just prior to YSL formation, the marginal blastomeres flattened towards the yolk cortex (note difference in curvature of marginal blastomeres between Fig. 1Dii and Fig. 1Cii). Cell boundaries were detected between some marginal blastomeres (Fig. 1Di, arrowheads), but not others (Fig. 1Di, arrow).

Midblastula transition (MBT) begins at this stage (Kane and Kimmel, 1993). MBT is characterized by initiation of zygotic transcription, cell cycle lengthening and loss of cell cycle synchrony (note some cells in interphase [Fig. 1Diii inset, arrow] and others in mitosis [Fig. 1Diii inset, arrowhead]). The YSL is formed at the end of the 512-cell stage, after the tenth mitosis (Kimmel and Law, 1985). At the 1k-cell stage, just after YSL formation, most marginal blastomeres have lost their boundaries, suggesting that pre-existing cell membranes recede. However, remnants of a few boundaries could still be detected (Fig. 1Ei, arrowheads). The microtubules of the newly formed YSL radiate from the yolk syncytial nuclei (YSN), forming large interdigitating aster-like arrays (Fig. 1Eii, arrowheads) (Solnica-Krezel and Driever, 1994). The yolk cortical microtubules now emanate from the YSL (i.e., the former marginal blastomeres) instead of the current marginal blastomeres. By the oblong stage (3.7 hpf), the YSN have divided several times (Kimmel et al., 1995) and spread vegetally (Fig. 1Fi, arrowhead), as well as beneath the blastoderm to form the internal-YSL (I-YSL) (Korzh et al., 1989; Solnica-Krezel and Driever, 1994). The YSL microtubule network now consists of a dense mat of intercrossing microtubules adjacent to the blastoderm and large astral-like assemblies radiating from the vegetal-most YSN (Fig. 1Fiii, dashed circle). The yolk cytoplasmic layer (YCL) microtubule array extends from these astral-like arrays of the vegetal YSN.

To better understand the membrane dynamics during YSL formation, time-lapse confocal microscopy was employed to visualize events at the blastoderm margin using the mGFP (membrane-targeted GFP) transgenic line, which expresses GFP fused with the last 20 amino acids of c-Ha-Ras, a sequence that provides farnesylation and palmitoylation signals for plasma membrane targeting, driven by the medaka β-actin promoter (Cooper et al., 2005). At the 512-cell stage, cell membranes of the marginal blastomeres are still evident (Fig. 2A, white arrowhead; supplementary material Movie 1). During the next division cycle, no new cleavage furrows form at the margin (Fig. 2G–N, arrow). Pre-existing cell membranes of the marginal blastomeres regress over the next cycle (Fig. 2M–R; supplementary material Movie 1, red arrowhead) and nuclei reappear after this mitosis sharing a common cytoplasm, thus forming the YSL. These events occur very quickly, giving the appearance of marginal blastomeres collapsing onto the yolk cell.

Disruption of the cytoskeleton induces YSL formation

Microtubules and microfilaments are dynamic components of the cell cytoskeleton. Both cytoskeletal elements are constantly being remodelled and redistributed within the cell. This dynamism is vital to the function of the cytoskeleton especially in the control
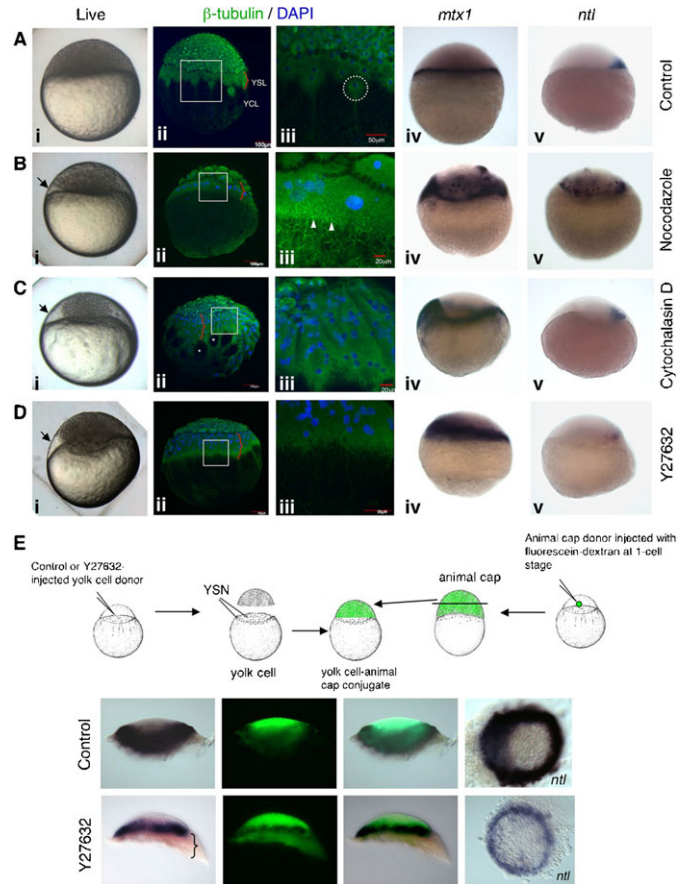
Fig. 1. Dynamics of yolk cortical microtubules and marginal blastomere boundaries during YSL formation. Whole-mount embryos were stained for β-tubulin (green), F-actin (red) and DNA (blue). All images are projections of multiple focal planes. Insets show higher magnifications of boxed areas in the respective panels. (**A**) The furrow microtubule array (FMA) between blastomeres (Aiii, arrowhead) is apparent at the 32-cell stage. (**B**) YCL microtubules of the marginal blastomeres at 128-cell stage. (**C**) 256-cell stage microtubule arrays extend into the YCL (Ciii inset, curly bracket). Arrowheads in Ai–Ci indicate prominent lower borders between marginal blastomeres. (**D**) Marginal blastomeres flattened at the 512-cell stage; some have lost cell borders (Di, arrow) while others are still present (Di, arrowheads). Arrow in Diii inset indicates a cell in interphase; arrowhead indicates a mitotic cell. (**E**) At 1k-cell stage, some marginal cell borders remain (Ei, arrowheads). Arrowheads in Eii indicate large interdigitating aster-like microtubule arrays. (**F**) At oblong stage, YSN have multiplied and spread vegetally (Fi, arrowhead). Dashed circle in Fiii highlights the microtubule arrays radiating from a vegetal YSN.
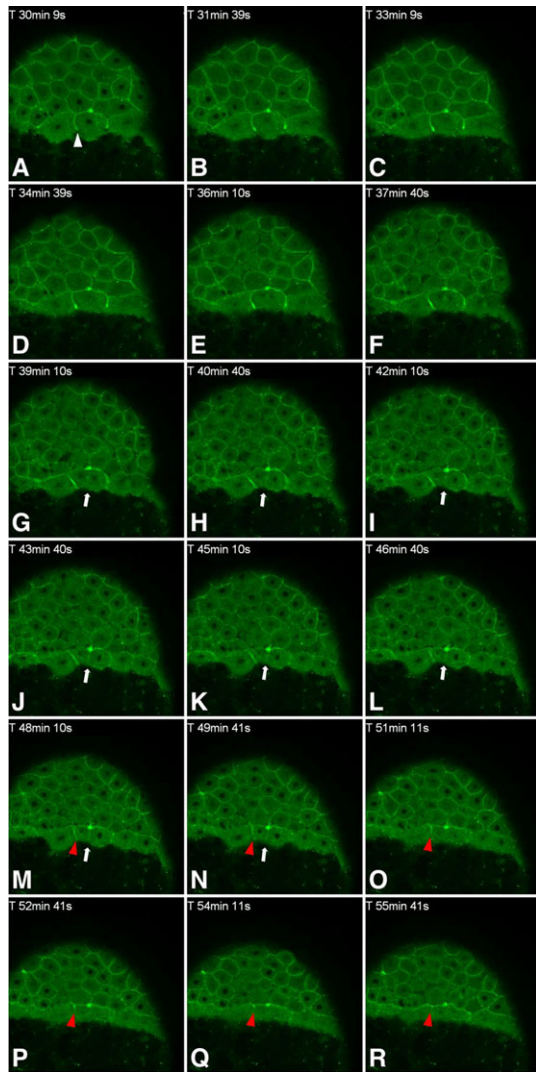
Fig. 2. *In vivo* membrane dynamics at the blastoderm edge during YSL formation during normal development. Selected frames from supplementary material Movie 1 showing the sequence of events during YSL formation. The prominent cell membrane of a marginal blastomere is obvious at the 512-cell stage (arrowhead in **A**). Note the absence of membrane between daughter nuclei as the cells divide to give rise to a 1k-cell stage embryo (white arrow in **G–N**). Note a pre-existing membrane at the margin regressing as the YSL develops (red arrowhead in **M–R**). Nuclei are unstained and appear as dark circles.

Fig. 3. **Disruption of cytoskeletal elements induces formation of enlarged YSL.** (**A**) Control, (**B**) nocodazole-treated, (**C**) cytochalasin D-treated, and (**D**) Y27632-injected embryos between oblong to sphere stages. Arrows in Bi–Di indicate enlarged YSL. Curly brackets in Aii–Dii indicate the width of the YSL microtubule belt. (Aiii–Diii) High magnification images of boxes in Aii–Dii respectively. (Aii,Aiii) Microtubule distribution in a control embryo. A large aster in the YSL (stippled circle, Aiii). (Bii,Biii) Disorganized microtubules in the YSL and YCL, with small asters in the enlarged YSL (arrowheads, Biii). (Cii,Ciii) Gaps in the YCL (Ciii, asterisks). (Dii,Diii) Dense YSL and sparse YCL microtubule arrays. The enlarged syncytia express *mtx1* (Biv–Div), and induces *ntl* in the overlying blastoderm (Bv–Dv). (**E**) Mesoderm induction assay. The enlarged syncytium (curly bracket) induced *ntl* in the fluorescein-labelled animal cap.

of cell division, cell shape and motility. To characterize the role of these elements in YSL formation, we tested the effects of the microtubule-depolymerizing drug, nocodazole, and the inhibitor of actin polymerization, cytochalasin D, on this process.

Consistent with a previous study (Jesuthasan and Strähle, 1997), nocodazole-treated embryos developed an enlarged syncytium (Fig. 3Bi, arrow) with small asters (Fig. 3Biii, arrowheads) instead of the large asters characteristic of normal YSL (Fig. 3Aiii, broken circle). The YCL microtubules of treated embryos were in disarray, lacking the animal-vegetal orientation of untreated embryos (compare Fig. 3Biii with Fig. 3Aiii). The enlarged syncytium expressed the YSL-specific marker *mtx1* (Fig. 3Biv) and could induce the pan-mesodermal marker *ntl* in the overlying blastoderm (Fig. 3Bv).

Cytochalasin D-treated embryos also developed an enlarged acellular region of cytoplasm (arrow in Fig. 3Ci), which contained dense disorganized microtubules without asters (Fig. 3Cii,Ciii). Some regions in the YCL were devoid of microtubules (Fig. 3Cii, asterisks). Again, the enlarged syncytium expressed *mtx1* (Fig. 3Civ) and induced *ntl* in the blastoderm above (Fig. 3Cv). The enzyme Rock is an upstream regulator of the actin cytoskeleton (Riento and Ridley, 2003). Y27632 is a specific inhibitor of the ROCK family of kinases. Its affinity for ROCKI and ROCKII as determined by Ki values was at least 20 to 30 times higher than those for two other Rho effector kinases, citron kinase and protein kinase PKN (Ishizaki et al., 2000). In order to determine whether it plays a role upstream of actin in this context, embryos at the 1-cell stage were injected with Y27632. Embryos injected with 2 pmol Y27632 developed enlarged syncytia similar to cytochalasin-treated embryos (Fig. 3Di, arrow) with dense disordered microtubules

(Fig. 3Dii,iii). In contrast, the YCL microtubules in Y27632-injected embryos appeared sparse in comparison to control YCL (compare Fig. 3Diii with Fig. 3Aiii). The enlarged syncytium in Y27632-injected embryos expressed *mtx1* (Fig. 3Div) and could induce *ntl* endogenously in the overlying blastoderm (Fig. 3Dv) as well as in animal caps (Fig. 3E) confirming the identity of this layer as the YSL. Together, the data suggest that disruption of cytoskeletal elements induces YSL formation, and the Rho-Rock signalling pathway is involved in this process.

Rock1, but not Rock2, is involved in YSL formation

Two ROCK isoforms have been identified in mammals – ROCKI/ROKβ and ROCKII/ROKα (Riento and Ridley, 2003). In zebrafish, only *rock2* paralogues have been cloned thus far: *rock2a*, which has been shown to be required for mediolateral cell elongation in convergence-extension movements during gastrulation (Marlow et al., 2002) and *rock2b*, which is necessary for establishing anteroposterior asymmetry of the Kupffer's vesicle (Wang et al., 2011). Unlike *rock2b*, *rock2a* is expressed maternally; hence, it may have a role prior to gastrulation. To determine whether zebrafish Rock2a is involved in YSL formation, dominant-negative Rock2a (dn-Rock2a) was generated by deletion of the amino terminus containing the kinase domain (Marlow et al., 2002) (Fig. 4A). Overexpression of *dn-rock2a* resulted in dose-dependent enlargement of cells with single enlarged nuclei in each cell (Fig. 4Cii′,ii″, arrowheads), which indicates failure of both karyokinesis and cytokinesis. Since cytokinesis and karyokinesis are temporally coordinated such that furrow ingression closely follows the segregation of chromosomes in anaphase, failure of cytokinesis in dn-Rock2a expressing cells could be a secondary consequence of karyokinesis failure. The YSL, however, appeared to have formed normally suggesting that Rock2a is not responsible for regulating the cytoskeletal dynamics leading to YSL formation.

Hence, we proceeded to clone zebrafish *rock1*. The predicted protein shares 80–90% identity with Rock1 from other teleosts (Fig. 5A). Interestingly, amino acid sequence identity between human ROCKI and ROCKII is 65.9%, whereas that between zebrafish Rock1 and Rock2a and Rock2b is slightly less (61.8% and 54.5%, respectively), implying a faster rate of divergence between the zebrafish Rocks. Transcripts of *rock1* are ubiquitously expressed during cleavage blastula and gastrula stages (Fig. 5Bi–iii). By 36hpf, expression is restricted to anterior structures, including the forebrain and hindbrain (Fig. 5Biv).

Similar to Y27632-injected embryos, dn-Rock1 expressing embryos developed an enlarged YSL with a disorganized microtubule network (Fig. 4Ciii′,iii″). Time-lapse confocal microscopy of mGFP embryos expressing dn-Rock1 revealed that nuclear division proceeds normally in the absence of cell membrane formation in the affected cells (Fig. 6; supplementary material Movie 2) (*n*=7). This occurs predominantly in the marginal cells (Fig. 6A–C; supplementary material Movie 2, white arrows) whereas cells near the animal pole are not affected as much (Fig. 6H–M; supplementary material Movie 2, arrowheads). Cell membranes of non-marginal cells that eventually syncytialize appear to regress after several rounds of nuclear division (Fig. 6D–R; supplementary material Movie 2, red arrow), suggesting that Rock1 activity is also required for prevention of furrow regression in addition to cleavage furrow formation during cytokinesis in the early zebrafish embryo. This is consistent with observations in other systems. In the *C. elegans* hypomorphic Rho-binding kinase mutant, *let-502 (sb106)*, some cells fail to complete cytokinesis: furrows initiate and ingress slightly but later regress (Piekny and Mains, 2002). In *Drosophila*, Rok has been shown to promote cleavage furrow ingression (Hickson et al., 2006); and in mammalian cells, preventing ROCK activation of myosin II by dissociating the septin scaffold that physically links the kinase to its substrate results in cleavage furrow regression (Joo et al., 2007).
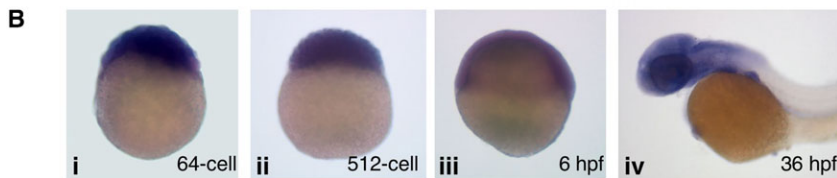
Our data suggest a model of YSL formation involving specific attenuation of Rock1 function at the blastoderm margin leading to localized and controlled cytokinesis failure. This could occur in response to a maternally expressed signal localized only to the blastoderm margin. Since Rock is inactivated directly by Gem (Ward et al., 2002) and indirectly by Rho-GAP (Riento and Ridley,
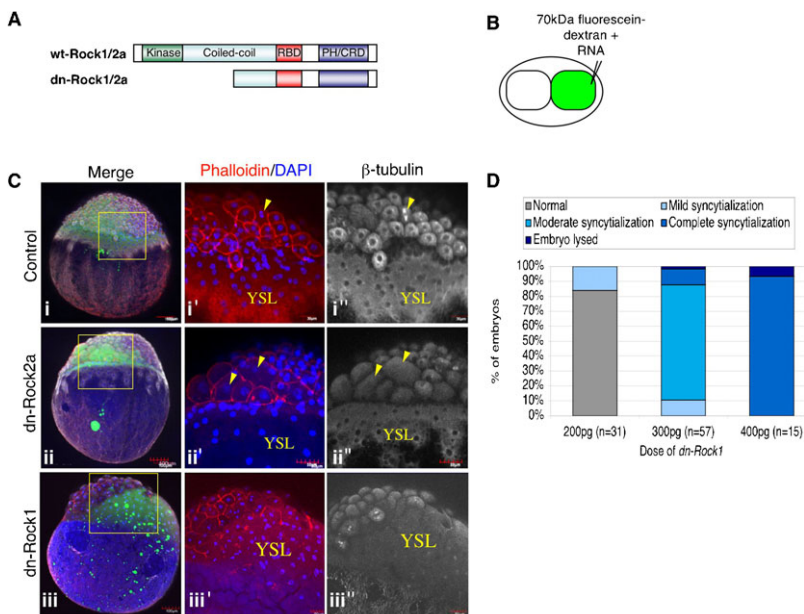
Fig. 4. Rock1, but not Rock2a, is necessary for YSL formation in the zebrafish embryo. (**A**) Protein domains of Rock1 and Rock2a and the putative dominant-negative (dn) construct. (**B**) Schematic of single-cell injection into the 2-cell stage embryo. (**C**) Embryos at oblong stage were stained for β-tubulin (white), F-actin (red) and DNA (blue). Images are projections of multiple focal planes. Arrowheads in Ci′,i″ indicate a mitotic cell in late anaphase. Injection of dn-Rock2a (Cii–ii″) did not affect YSL formation. Injection of dn-Rock1 (Ciii–iii″) caused expansion of the YSL. (**D**) Statistical data for embryos expressing dn-Rock1 showing dose-dependent YSL expansion.

A

B
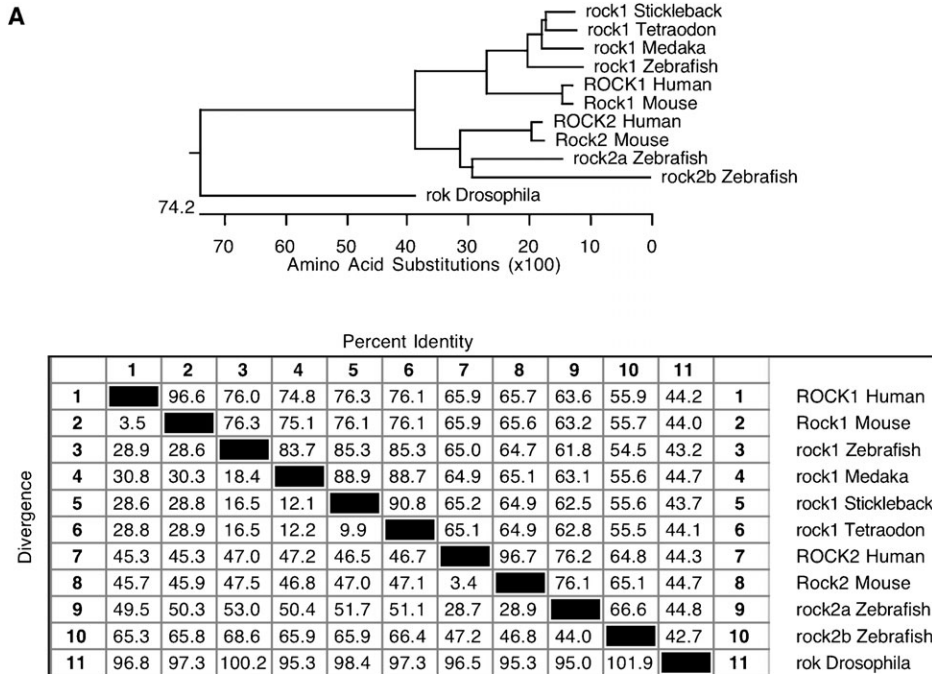
Fig. 5. **Cloning of *rock1* and its expression pattern during development.** (**A**) Multiple amino acid sequences were aligned using ClustalW algorithm. Calculation of sequence similarity and distance as well as phylogeny reconstruction were done using MegAlign from DNASTAR Lasergene v8.0.2. Full-length amino acid sequences were retrieved either from Ensembl database (Zv9, release 63), ENSORLP00000022079 (medaka Rock1), ENSGACP00000022893 (stickleback Rock1), ENSTNIP00000001304 (tetraodon Rock1), FBpp0074061 (Drosophila Rok) or from NCBI database, NP_005397.1 (human ROCK1), NP_033097.1 (mouse ROCK1), NP_004841.1 (human ROCK2), NP_033098.1 (mouse ROCK2), AAK97854.1 (zebrafish Rock2a), CAI21196.1 (zebrafish Rock2b). (**B**) Early *rock1* mRNA is of maternal origin. It is expressed ubiquitously at (Bi) 64-cell, (Bii) 512-cell, and (Biii) 6 hpf. (Biv) At 36 hpf, *rock1* is detected in anterior structures, including forebrain and hindbrain.

Percent Identity

Divergence	1	2	3	4	5	6	7	8	9	10	11		
1		96.6	76.0	74.8	76.3	76.1	65.9	65.7	63.6	55.9	44.2	1	ROCK1 Human
2	3.5		76.3	75.1	76.1	76.1	65.9	65.6	63.2	55.7	44.0	2	Rock1 Mouse
3	28.9	28.6		83.7	85.3	85.3	65.0	64.7	61.8	54.5	43.2	3	rock1 Zebrafish
4	30.8	30.3	18.4		88.9	88.7	64.9	65.1	63.1	55.6	44.7	4	rock1 Medaka
5	28.6	28.8	16.5	12.1		90.8	65.2	64.9	62.5	55.6	43.7	5	rock1 Stickleback
6	28.8	28.9	16.5	12.2	9.9		65.1	64.9	62.8	55.5	44.1	6	rock1 Tetraodon
7	45.3	45.3	47.0	47.2	46.5	46.7		96.7	76.2	64.8	44.3	7	ROCK2 Human
8	45.7	45.9	47.5	46.8	47.0	47.1	3.4		76.1	65.1	44.7	8	Rock2 Mouse
9	49.5	50.3	53.0	50.4	51.7	51.1	28.7	28.9		66.6	44.8	9	rock2a Zebrafish
10	65.3	65.8	68.6	65.9	65.9	66.4	47.2	46.8	44.0		42.7	10	rock2b Zebrafish
11	96.8	97.3	100.2	95.3	98.4	97.3	96.5	95.3	95.0	101.9		11	rok Drosophila

2003), they are potential targets for this maternal signal. Another possible model of YSL formation was recently proposed by Takesono and colleagues, in which solute carrier family 3 member 2 (Slc3a2) inhibits RhoA/Rock signalling via c-Src activation, thereby regulating microtubule dynamics and YSL organization (Takesono et al., 2012). They reported that Slc3a2 knockdown caused YSL expansion, which was rescued by treatment with Y27632. The likely explanation for the apparent discrepancy between our results is that the level of Rock activity at the margin needs to be within an acceptable range for normal YSL formation – any deviation from this range in either direction results in YSL expansion. Our hypothesis that attenuation of Rock1 activity is necessary for YSL formation is consistent with the proposed Slc3a2-mediated signalling pathway, and implicates Rock1, but not Rock2, as the effector of RhoA signalling in this pathway.

Maternal-effect mutants that have defects in the cytokinetic machinery such as *cellular island* (*cei*), which affects Aurora-B kinase (Yabe et al., 2009), and *cellular atoll* (*cea*), which affects the centriolar protein Sas-6 (Yabe et al., 2007), also develop an expanded YSL (supplementary material Fig. S1), lending support to the hypothesis that YSL formation is a result of cytokinesis failure. Indeed, this mechanism of controlled cytokinesis failure or abortive cytokinesis has been employed in mammalian developmental programs such as cardiomyocyte binucleation (Engel et al., 2006), hepatocyte tetraploidization (Margall-Ducos et al., 2007), and megakaryocyte polyploidization (Lordier et al., 2008). Understanding how cytokinesis is aborted in these

physiological settings would expand our understanding of how cytokinesis fails in pathological states such as cancer.

Materials and Methods

Zebrafish husbandry

Wild-type zebrafish (AB strain), transgenic and mutant lines were maintained as described (Westerfield, 2000) in accordance with IACUC regulations (Biopolis IACUC application NO. 050096). All embryos were generated by pair-wise matings and staged according to Kimmel and colleagues (Kimmel et al., 1995).

Embryo stainings

Whole-mount *in situ* hybridization, immunohistochemistry and cryosectioning were performed as described (Korzh et al., 1993; Korzh et al., 1998). KMX-1 (Solnica-Krezel and Driever, 1994) (Chemicon) and secondary goat anti-mouse IgG-Alexa-488/Alexa-633 (Molecular Probes) were used to detect β-tubulin. Alexa-546-phalloidin (Molecular Probes) was used at 66 nM for fluorescent labelling of actin. DNA was labelled by incubating embryos in 0.3 μM DAPI (Sigma).

Drug treatments

Embryos in their chorions were incubated in 0.1 μg/ml nocodazole (10 mg/ml stock in DMSO) from the 16-cell stage to 4 hpf. For cytochalasin D, embryos in their chorions were incubated in 15 μg/ml (5 mg/ml stock in DMSO) for 35 minutes from the 2–4 cell stage, then washed and left to develop until sphere stage in embryo medium. Y27632 (Calbiochem) was prepared as a 30 mM stock in DMSO. All drugs were diluted to the appropriate concentrations in embryo medium prior to use. Controls were performed by treating sibling embryos in the same manner with the corresponding concentration of solvent in embryo medium.

Cloning of full-length *rock1*

RNA was isolated from 2 hpf embryos using RNA Purification Kit (QIAGEN). First-strand cDNA was synthesized by oligo(dT) priming using PowerScript reverse transcriptase (Clontech). To determine the 5′-end of *rock1*, we performed
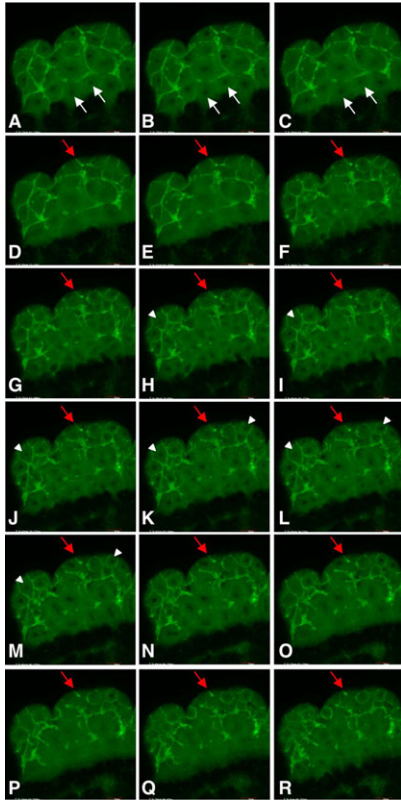
Fig. 6. *In vivo* **membrane dynamics at the blastoderm edge during YSL formation upon injection of** *dn-rock1*. Selected frames from supplementary material Movie 2 showing the sequence of membrane failure events in a representative dn-Rock1 expressing embryo. Note the lack of membrane deposition between marginal nuclei (white arrows in **A–C**). Most cells near the animal pole undergo normal nuclear and cell division (arrowheads in **H–M**). Note the regression of cell membranes in a syncytializing non-marginal cell after multiple rounds of nuclear division (red arrow in **D–R**).

5′-RACE PCR (SMART RACE cDNA Amplification Kit from Clontech) with gene-specific primers (5′-ACA ACC TCC GCA GTG TAG AAG CGT G-3′ and 5′-TGC TGA GCA GCT TCA TGG CGT AGA C-3′). Full-length cDNA of *rock1* was amplified using Expand Long Template PCR System (Roche). Gene-specific primers (5′-GAA GGC GGA CAT GTT GGT CGG GCA G-3′ and 5′-TGT GTC GTC CGA ACA GAA CAG CTG A-3′) were designed based on sequence derived from 5′-RACE and Ensembl database (Zv8). The PCR product of approximately 5.2 kb was cloned into pGEM-T Easy vector (Promega). The sequence information for the complete *rock1* mRNA was deposited into GenBank (Acc. no. JN416777). *dn-rock2a* was generated according to Marlow and colleagues (Marlow et al., 2002). *dn-rock1* was amplified by PCR from full-length *rock1* using modified primers to introduce *Bgl*II (5′-GCA GAT CTC GAT GGA GAA AGA CTC CAC CAT-3′) and *Spe*I (5′-GCA CTA GTT GCA GAG GAC AGT ACA AAA TCC-3′) sites and subcloned into pT7TS vector (Johnson and Krieg, Austin, UT).

RNA injections
5′-capped sense RNA was synthesized with the mMessage mMachine T7 kit (Ambion). RNA was injected into a single blastomere at the 2-cell stage. Doses injected ranged from 93–1800 pg of *dn-rock2a* and 200–400 pg of *dn-rock1*.

Generation of yolk cell-animal cap conjugates
The mesoderm induction assay was performed as described by Ober and Schulte-Merker (Ober and Schulte-Merker, 1999).

Microscopy
Observation of live embryos was performed using either SZX12 dissecting microscope (Olympus) or Fluoview FV1000 confocal system attached to an inverted microscope (Olympus IX81). Immunofluorescence-stained embryos were imaged by confocal microscopy (Fluoview FV1000 attached to upright Olympus BX61microscope).

References
Carvalho, L. and Heisenberg, C. P. (2010). The yolk syncytial layer in early zebrafish development. *Trends Cell Biol.* **20**, 586-592.

Cooper, M. S., Szeto, D. P., Sommers-Herivel, G., Topczewski, J., Solnica-Krezel, L., Kang, H. C., Johnson, I. and Kimelman, D. (2005). Visualizing morphogenesis in transgenic zebrafish embryos using BODIPY TR methyl ester dye as a vital counterstain for GFP. *Dev. Dyn.* **232**, 359-368.

Eggert, U. S., Mitchison, T. J. and Field, C. M. (2006). Animal cytokinesis: from parts list to mechanisms. *Annu. Rev. Biochem.* **75**, 543-566.

Engel, F. B., Schebesta, M. and Keating, M. T. (2006). Anillin localization defect in cardiomyocyte binucleation. *J. Mol. Cell. Cardiol.* **41**, 601-612.

Etienne-Manneville, S. and Hall, A. (2002). Rho GTPases in cell biology. *Nature* **420**, 629-635.

Hickson, G. R., Echard, A. and O'Farrell, P. H. (2006). Rho-kinase controls cell shape changes during cytokinesis. *Curr. Biol.* **16**, 359-370.

Ishizaki, T., Uehata, M., Tamechika, I., Keel, J., Nonomura, K., Maekawa, M. and Narumiya, S. (2000). Pharmacological properties of Y-27632, a specific inhibitor of rho-associated kinases. *Mol. Pharmacol.* **57**, 976-983.

Jesuthasan, S. and Strähle, U. (1997). Dynamic microtubules and specification of the zebrafish embryonic axis. *Curr. Biol.* **7**, 31-42.

Joo, E., Surka, M. C. and Trimble, W. S. (2007). Mammalian SEPT2 is required for scaffolding nonmuscle myosin II and its kinases. *Dev. Cell* **13**, 677-690.

Kane, D. A. and Kimmel, C. B. (1993). The zebrafish midblastula transition. *Development* **119**, 447-456.

Kimmel, C. B. and Law, R. D. (1985). Cell lineage of zebrafish blastomeres. II. Formation of the yolk syncytial layer. *Dev. Biol.* **108**, 86-93.

Kimmel, C. B., Ballard, W. W., Kimmel, S. R., Ullmann, B. and Schilling, T. F. (1995). Stages of embryonic development of the zebrafish. *Dev. Dyn.* **203**, 253-310.

Korzh, V., Baikova, O. and Dmitrevskaya, T. (1989). Microinjection of fluorescent dyes into loach embryos. II. Studies of morphology of giant nuclei of yolk syncytial layer. *Ontogenez* **20**, 357-363.

Korzh, V., Edlund, T. and Thor, S. (1993). Zebrafish primary neurons initiate expression of the LIM homeodomain protein Isl-1 at the end of gastrulation. *Development* **118**, 417-425.

Korzh, V., Sleptsova, I., Liao, J., He, J. and Gong, Z. (1998). Expression of zebrafish bHLH genes ngn1 and nrd defines distinct stages of neural differentiation. *Dev. Dyn.* **213**, 92-104.

Lordier, L., Jalil, A., Aurade, F., Larbret, F., Larghero, J., Debili, N., Vainchenker, W. and Chang, Y. (2008). Megakaryocyte endomitosis is a failure of late cytokinesis related to defects in the contractile ring and Rho/Rock signaling. *Blood* **112**, 3164-3174.

Margall-Ducos, G., Celton-Morizur, S., Couton, D., Brégerie, O. and Desdouets, C. (2007). Liver tetraploidization is controlled by a new process of incomplete cytokinesis. *J. Cell Sci.* **120**, 3633-3639.

Marlow, F., Topczewski, J., Sepich, D. and Solnica-Krezel, L. (2002). Zebrafish Rho kinase 2 acts downstream of Wnt11 to mediate cell polarity and effective convergence and extension movements. *Curr. Biol.* **12**, 876-884.

Mizuno, T., Yamaha, E., Wakahara, M., Kuroiwa, A. and Takeda, H. (1996). Mesoderm induction in zebrafish. *Nature* **383**, 131-132.

Mizuno, T., Yamaha, E., Kuroiwa, A. and Takeda, H. (1999). Removal of vegetal yolk causes dorsal deficencies and impairs dorsal-inducing ability of the yolk cell in zebrafish. *Mech. Dev.* **81**, 51-63.

Ober, E. A. and Schulte-Merker, S. (1999). Signals from the yolk cell induce mesoderm, neuroectoderm, the trunk organizer, and the notochord in zebrafish. *Dev. Biol.* **215**, 167-181.

Piekny, A. J. and Mains, P. E. (2002). Rho-binding kinase (LET-502) and myosin phosphatase (MEL-11) regulate cytokinesis in the early Caenorhabditis elegans embryo. *J. Cell Sci.* **115**, 2271-2282.

Riento, K. and Ridley, A. J. (2003). Rocks: multifunctional kinases in cell behaviour. *Nat. Rev. Mol. Cell Biol.* **4**, 446-456.

Rodaway, A., Takeda, H., Koshida, S., Broadbent, J., Price, B., Smith, J. C., Patient, R. and Holder, N. (1999). Induction of the mesendoderm in the zebrafish germ ring by yolk cell-derived TGF-beta family signals and discrimination of mesoderm and endoderm by FGF. *Development* **126**, 3067-3078.

Sakaguchi, T., Kikuchi, Y., Kuroiwa, A., Takeda, H. and Stainier, D. Y. (2006). The yolk syncytial layer regulates myocardial migration by influencing extracellular matrix assembly in zebrafish. *Development* **133**, 4063-4072.

Solnica-Krezel, L. and Driever, W. (1994). Microtubule arrays of the zebrafish yolk cell: organization and function during epiboly. *Development* **120**, 2443-2455.

Biology Open

Strähle, U. and Jesuthasan, S. (1993). Ultraviolet irradiation impairs epiboly in zebrafish embryos: evidence for a microtubule-dependent mechanism of epiboly. *Development* **119**, 909-919.

Takesono, A., Moger, J., Farooq, S., Cartwright, E., Dawid, I. B., Wilson, S. W. and Kudoh, T. (2012) Solute carrier family 3 member 2 (Slc3a2) controls yolk syncytial layer (YSL) formation by regulating microtubule networks in the zebrafish embryo. *Proc. Natl. Acad. Sci. USA* **109**, 3371-3376.

Trinkaus, J. P. (1993). The yolk syncytial layer of Fundulus: its origin and history and its significance for early embryogenesis. *J. Exp. Zool.* **265**, 258-284.

Walzer, C. and Schönenberger, N. (1979a). Ultrastructure and cytochemistry of the yolk syncytial layer in the alevin of trout (Salmo fario trutta L. and Salmo gairdneri R.) after hatching. II. The cytoplasmic zone. *Cell Tissue Res.* **196**, 75-93.

Walzer, C. and Schönenberger, N. (1979b). Ultrastructure and cytochemistry study of the yolk syncytial layer in the alevin of trout (Salmo fario trutta L.) after hatching. I. The vitellolysis zone. *Cell Tissue Res.* **196**, 59-73.

Wang, G., Cadwallader, A. B., Jang, D. S., Tsang, M., Yost, H. J. and Amack, J. D. (2011). The Rho kinase Rock2b establishes anteroposterior asymmetry of the ciliated Kupffer's vesicle in zebrafish. *Development* **138**, 45-54.

Ward, Y., Yap, S. F., Ravichandran, V., Matsumura, F., Ito, M., Spinelli, B. and Kelly, K. (2002). The GTP binding proteins Gem and Rad are negative regulators of the Rho-Rho kinase pathway. *J. Cell Biol.* **157**, 291-302.

Westerfield, M. (2000). *The Zebrafish Book: A Guide For The Laboratory Use Of Zebrafish (Danio Rerio)*. 5th edn. Eugene, OR, USA: University of Oregon Press.

Yabe, T., Ge, X. and Pelegri, F. (2007). The zebrafish maternal-effect gene cellular atoll encodes the centriolar component sas-6 and defects in its paternal function promote whole genome duplication. *Dev. Biol.* **312**, 44-60.

Yabe, T., Ge, X., Lindeman, R., Nair, S., Runke, G., Mullins, M. C. and Pelegri, F. (2009). The maternal-effect gene cellular island encodes aurora B kinase and is essential for furrow formation in the early zebrafish embryo. *PLoS Genet.* **5**, e1000518.